Microchimica Acta (2020) 187:575
https://doi.org/10.1007/s00604-020-04548-5

ORIGINAL PAPER

A label-free electrochemical biosensor based on magnetic biocomposites with DNAzyme and hybridization chain reaction dual signal amplification for the determination of Pb^{2+}

Chenyuan Weng[1] · Xiaoyun Li[1] · Qiaoyun Lu[1] · Wei Yang[1] · Jing Wang[1] · Xiaoqiang Yan[1] · Bingzhi Li[2] · Marwan Sakran[1] · Junli Hong[1] · Wanying Zhu[1] · Xuemin Zhou[1]

Received: 23 May 2020 / Accepted: 2 September 2020

Abstract

A highly sensitive and selective electrochemical biosensor for Pb^{2+} with a dual-amplification strategy is proposed. The first amplification step was realized by the cycle of Pb^{2+} and 8–17 DNAzyme (S2), and the hybridization chain reaction (HCR) triggered by S1 further amplified the electrochemical signal. Fe_3O_4@Au NPs, as a multifunctional magnetic carrier, is not only manifested in the construction of a magnetically controlled electrochemical response interface, but also has significant contribution in the purifying system, reducing interference, increasing the specific surface area, and the DNA loading. The magnetic nanocomposites were characterized by TEM as spheres with particle size of around 39 nm. When there was no Pb^{2+}, long double-strand DNA (dsDNA) is formed on the surface of Fe_3O_4@Au NPs by the S1-triggered HCR; in the presence of Pb^{2+}, S2 is activated and S1 on the surface of magnetic biocomposites (Fe_3O_4@Au NPs-S1) is continuously cleaved with the cycle of Pb^{2+} and S2, leading to a significant decrease of methylene blue (MB) absorbed on dsDNA. Such reverse dual-signal amplification strategy effectively increased the current difference and improved the sensitivity of the proposed sensor. The electrochemical signal of MB was obtained by differential pulse voltammetry (DPV) with preconcentration, showing a linear response toward Pb^{2+} ranging from 50 pM to 1 μM with a detection limit of 15 pM. The proposed method has feasible applications in detecting other heavy metal ions based on other metal-dependent DNAzyme.

Keywords Dual amplification · Label-free detection · Multifunctional magnetic carrier · Pb^{2+} determination · Environmental monitoring

Introduction

Heavy metal pollution is an important factor leading to environmental deterioration [1, 2]. Even trace amounts of heavy metal pollution into the human body will cause great harm to the human body [3]. Lead ion (Pb^{2+}) is one of the most toxic heavy metal ions that can induce various serious diseases, including neurological disorders, cardiovascular disease, and memory lapses [4, 5]. Considering its severe toxicity, World Health Organization (WHO) has set the highest allowable limit for Pb^{2+} in drinking water at 48 nM [6]. Therefore, it is significant to develop a highly sensitive and reliable method for Pb^{2+} determination.

Over the past years, various analysis techniques have been utilized in detecting Pb^{2+}, such as atomic absorption spectrometry (AAS) [7], X-ray fluorescence spectrometry (XRF) [8], inductively coupled plasma mass spectrometry (ICP-MS) [9], et al. These determination techniques usually require expensive determination instruments and have poor portability. In recent years, researchers have developed various novel sensing systems for Pb^{2+} determination, including colorimetric, fluorometric, and electrochemical techniques [10–12]. Among them,

Electronic supplementary material The online version of this article (https://doi.org/10.1007/s00604-020-04548-5) contains supplementary material, which is available to authorized users.

✉ Wanying Zhu
wanyingzhu@njmu.edu.cn

✉ Xuemin Zhou
xueminzhou001_001@hotmail.com

[1] School of Pharmacy, Nanjing Medical University, Nanjing 211166, Jiangsu, China

[2] School of Food Science and Pharmaceutical Engineering, Nanjing Normal University, Nanjing 210023, China

Published online: 24 September 2020

electrochemical sensors show outstanding strengths such as convenient operation, rapid determination, high sensitivity, and the possible portability [13–15]. In order to improve the selectivity of electrochemical sensor, 8–17 DNAzyme which is specific single-strand sequence is used as molecular recognition elements, showing high catalytic activity and good selectivity towards Pb^{2+} [16]. When there is Pb^{2+}, the DNAzyme could be activated so that the substrate strand could be split into two fragments at the ribonucleoside adenosine (rA) position.

Fe_3O_4@Au NPs exhibited obvious advantages in the performance of the electrochemical sensor. Fe_3O_4@Au NPs can be distributed quickly and regularly on the magnetic glassy carbon electrode (MGCE) surface by magnetic field-directed self-assembly [17–20]; a soft-modified electrochemical magneto-controlled response interface was constructed. When the magnetic core was removed after measurement, the response interface on the surface of the electrode can fall off. Here, the complex electrode modification was eliminated and the regeneration of the electrode was simplified. In addition, Fe_3O_4@Au NPs can be easily modified and assembled with DNA by Au–S bonds, and large capacity was provided for modifiers with their large specific surface area [19, 21, 22].

The HCR is an initiator-triggered reaction, using a trigger strand of DNA to cause two stable DNA hairpins to alternately recognize each other and hybridize to form DNA polymers with nicked double helices [23]. HCR is an enzyme-free, isothermal, and easy control amplification method, which does not require hybridization equipment [24], leading to a widespread application for constructing the sensing platform. Chu et al. developed a catalytic hairpin assembly/hyperbranched hybridization chain reaction-based photoelectrochemical sensor for human telomerase RNA, realizing the signal output through the H_2O_2 catalysis with the abundant DNAzyme of hemin/G-quadruplex [25]. Chen et al. proposed an ultrasensitive electrochemical biosensor in detecting DNA methylation with HCR amplification; H_2O_2 could be catalyzed by avidin-HRP which attached to DNA polymers through the biotin tagged on hairpin, realizing the signal output [26]. Herein, methylene blue (MB) as a redox indicator, which can easily interact with double-strand DNA (dsDNA) based on π–π stacking interactions, or single-stranded DNA (ssDNA) based on electrostatic adsorption [27–29], is used as a remarkable electrochemical signal probe in signal transformation [30–32].

Based on the above considerations, a highly sensitive and selective electrochemical biosensor for Pb^{2+} was designed based on a dual-amplification strategy. Firstly, the Pb^{2+} and DNAzyme (S2) could be circularly participated into the process of cutting substrate strand (S1), and the electrochemical signal be continuously reduced. Secondly, long-chain dsDNA could be formed with the uniquely designed S1 by the HCR. The transformation between Pb^{2+} and electrochemical signal molecules was realized by MB adsorbed on long dsDNA. This proposed electrochemical biosensor can be used for analyzing environmental water samples.

Materials and methods

Reagents and materials

Chloroauric acid ($HAuCl_4$), $FeCl_3{\cdot}6H_2O$, $FeCl_2{\cdot}4H_2O$, $NH_3{\cdot}H_2O$, (3-Ami-nopropyl) triethoxysilane (APTES), ethylenediamine tetraacetic acid (EDTA), boric acid, and sodium borohydride ($NaBH_4$) were purchased from Sinopharm Chemical Reagent (Shanghai, China, http://www.sinoreagent.com/). 6-Mercapto-1-hexanol (MCH) was supplied by Aladdin (Shanghai, China, http://www.aladdin-e.com/). Tris and DNA marker A (25~500 bp) was purchased from Sangon Biotech (Shanghai, China, http://www.sangon.com/). All oligonucleotide sequences were synthesized and purified by Sangon Biotech (Shanghai, China, http://www.sangon.com/) and are shown in Table S1. A Tris-HCl buffer 1 (10 mM trishydroxymethyl aminomethane hydrochloride (Tris-HCl), 100 mM NaCl (pH 7.4)) was used to dissolve the S1, S2. A Tris-HCl buffer 2 consisting of 10 mM Tris-HCl, and 10 mM NaCl (pH 7.4) was used to dissolve the hairpin oligonucleotides (H1 and H2) and employed as test solution for the electrochemical measurements. The H1 and H2 were acquired by heating up solution to 95 °C and maintaining for 5 min, then cooled to normal temperature gradually for at least 2 h. All other reagents used were of analytical grade, and no further purification was needed.

Instruments and characterizations

All electrochemical analyses were carried out using an electrochemical analyzer (CHI 660D, China). A conventional three-electrode system consisted of a platinum electrode as the counter electrode, a saturated calomel electrode (SCE) as the reference electrode, and a magnetic glassy carbon electrode (MGCE, Φ = 5 mm) as the working electrode. MGCE containing a demountable magnet was purchased from Tianjin Incole Union Technology (Tianjin, China, http://www.incole.com/). Transmission electron microscopy (JEOL, Japan, https://www.jeol.co.jp/) was conducted to obtain images. The UV–Vis absorption spectroscopy was recorded using a UV-2550 spectrophotometer (Shimazu, Japan, https://www.shimadzu.com.cn/). Gel electrophoresis used in 15% native-PAGE gel

(gel which could separate bases ranging from 25 to 150) with Tris-borate-EDTA (TBE buffer, containing Tris, boric acid, and EDTA) was obtained from Macklin Chemical (Shanghai, China, http://www.macklin.cn/), and gel image was photographed by 3500R Gel Image System (Shanghai, China, http://www.biotanon.com/).

Preparation of Fe_3O_4 NPs and Fe_3O_4@Au NPs

Firstly, Fe_3O_4 was synthesized using the one-step solvothermal method 17. $FeCl_3{\cdot}6H_2O$ of 4.70 g was dissolved in 80 mL ultrapure water and heated with stirring, 1.72 g $FeCl_2{\cdot}4H_2O$ was added when the temperature reached 80 °C under the protection of nitrogen, and 10 mL aqueous ammonia was dropwise added until the pH up to 10. The obtained Fe_3O_4 NPs was separated using a magnet after 30 min of reaction and washed three times with ethanol and then with water. The Fe_3O_4 NPs was finally dispersed in ultrapure water and preserved at 0–4 °C. Herein, 1 mL of the Fe_3O_4 NP suspension was taken and vacuum dried overnight; the concentration of the suspension was calculated to be 14 mg mL^{-1}. The Fe3O4@Au NPs were synthesized as follows. The 172-μL Fe_3O_4 NP suspension was shook in 20 mL of 10% (*v*/*v*) APTES absolute ethanol overnight, washed with ethanol and water, and dispersed in 30 mL water. Afterward, 0.72-mL aqueous solution of $HAuCl_4$ (48.5 mM) was added; then, 0.6-mL freshly prepared NaBH4 solution (25 mM) as reductant was added dropwise into the above solution with stirring for 5 min. The final Fe_3O_4@Au NPs were separated through external magnetic field and washed with ultrapure water for three times. According to the same quantitative method as Fe_3O_4 NPs, the concentration of Fe_3O_4@Au NPs was calculated to be 1.2 mg mL^{-1}.

Preparation of magnetic biocomposites

The obtained Fe_3O_4@Au NPs were added into a solution which contains 0.3 μM thiolated S1 in 10 mM Tris-HCl buffer (pH 7.4, 100 mM NaCl) and then stirred for 2 h. The Fe_3O_4@Au NPs-S1 were then shaken in 1 mM MCH for 1 h at room temperature to reduce non-specific adsorption.

Fabrication of electrochemical biosensor

The preparation process of the biosensor is illustrated in Scheme 1. The obtained Fe_3O_4@Au NPs-S1 was incubated in a mixture of 0.3 μM S2 and Pb^{2+} of different concentrations in 1-mL Tris-HCl buffer system for 40 min at 37 °C. After magnetic separation, a mixture solution of H1 and H2 was added into the reaction system for 90 min at 37 °C. After that, 100 μM MB was added and stirred for 20 min, realizing the interaction with DNA. Finally, the resulting biocomposites were washed with Tris-HCl buffer to remove any excess MB and diffused in 2-mL Tris-HCl buffer, a MGCE was inserted into the surface of the buffer gently and vertically, realizing the adsorption of biocomposites on the surface of MGCE; the entire magnetic adsorption process took 5 min and the electrochemical signal was obtained by differential pulse voltammetry (DPV).

Results and discussion

Design of strategy

The constructed electrochemical biosensor for Pb^{2+} determination is schematically clarified in Scheme 1. The uniquely

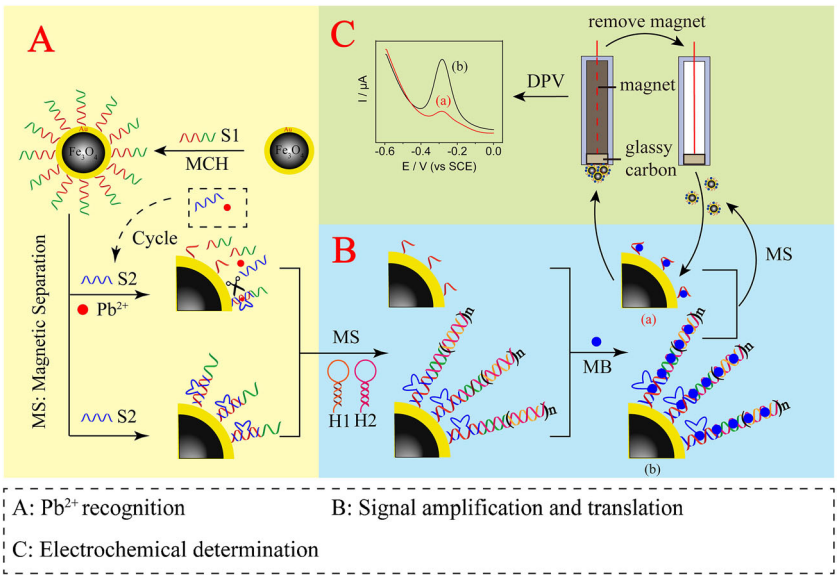

Scheme 1 Schematic illustration of the biosensor for the Pb^{2+} determination.

designed S1 was used for signal amplification by HCR and the S2 was used as a selective recognition element. The substrate S1 was consisted of the Pb^{2+} action site rA and the HCR trigger sequence which could initiate a HCR reaction. The substrate S1 could be firmly anchored on Fe_3O_4@Au NPs by the Au–S interaction. After that, the excess sites which were not occupied by S1 were removed by the MCH fixed to the surface of the Fe_3O_4@Au NPs-S1 by the Au–S interaction between MCH and Au. When there is Pb^{2+}, the S2 was activated and the S1 would be cleaved; the HCR trigger sequence was fall off. As a result, the S1 only left residual DNA fragment immobilized on the Fe_3O_4@Au NPs. In the absence of Pb^{2+}, the substrate S1 could not be cleaved. Thus, the HCR trigger sequence at the 3′ terminal of S1 could initiate the following HCR reaction after the addition of H1 and H2. After that, long dsDNA were formed on the surface of Fe_3O_4@Au NPs. Ultimately, a mass of signal probe MB was absorbed on the long dsDNA based on π–π stacking interactions, generating an obvious electrochemical response. The quantitative determination of Pb^{2+} was realized by detecting the electrochemical signal of MB on DNA.

Three times of magnetic separation were involved in the experiment (Scheme 1): for the first time, the free S1 was separated to avoid the cleavage of free S1 by Pb^{2+}; secondly, the HCR trigger sequence was separated from the reaction system and HCR could not occur; for the last time, the excess MB was removed to eliminate the interference of excess MB on the determination results.

The proposed electrochemical biosensor for Pb^{2+} contained three amplification elements. Firstly, the Pb^{2+} and the S2 were able to circularly participate into cleaving the substrate S1, continually decreasing the I_T (I_T was electrochemical signal with adding Pb^{2+}). Secondly, the signal amplification function of HCR obviously increased the I_0 (I_0 was electrochemical signal without adding Pb^{2+}). Thus, the current difference value ($\Delta I = I_0 - I_T$) significantly increased after adding Pb^{2+}. Thirdly, the large specific surface area was provided for the immobilization of DNA by Fe_3O_4@Au NPs, and the electrochemical response of MB was further enhanced.

Choice of materials

Fe_3O_4@Au NPs were chosen as the material to construct the electrode interface. Comparing with simple Fe_3O_4 nanoparticles (curve b), the Au shell coated onto the Fe_3O_4 surface not only increased the amount of immobilization of DNA, but also enhanced the conductivity of the composite material (curve c), improving the current response (Fig. 1A). The magnetization curves (Fig. 1B) of VSM analysis showed that the saturation magnetization of Fe_3O_4 NPs (curve a) and Fe_3O_4@Au NPs (curve b) was about 60 emu g^{-1} and 47 emu g^{-1}, respectively. The gold nanoparticles on the surface of Fe_3O_4 NPs were most likely to cause a decrease in the saturation magnetization. There was no significant influence on the magnetic adsorption of Fe_3O_4@Au NPs to the electrode surface. The magnetic biocomposites could be rapidly adsorbed to the MGCE surface when a MGCE touched the surface of the test solution (about 30 s) as the inset in Fig. 1B shows. Taking advantage of the magnetism of Fe_3O_4@Au NPs, necessary purification and removal of interference signal can be realized by rapid magnetic separation. More importantly, free modification of electrode could be achieved by the introduction of Fe_3O_4@Au NPs, which reduce the batch-to-batch variation caused by electrode modification, saving the time of modifying and polishing the electrode compared with other electrochemical sensors (Table S2).

Characterization of Fe_3O_4@Au NPs

Figure 2 A exhibits the XRD spectra of Fe_3O_4 NPs and Fe_3O_4@Au NPs. The peaks of curve a at 2θ values of 30.2°, 35.6°, 43.2°, 53.6°, 57.3°, and 62.7° were typically XRD patterns (220), (311), (400), (422), (511), and (440), agreeing with that of the standard Fe_3O_4 [33, 34]. The peaks of Fe_3O_4@Au NPs at 35.5°, 44.3°, 64.5°, 77.7°, and 82.0° correspond with the crystal plane of AuNPs in (111), (200), (220), (311), and (222) [35]. The shape and dispersion of the nanoparticles were characterized with TEM. As shown in Fig. S1A and Fig. S1B, both the two kinds of nanoparticles were spherical in structure. The diameters of nanoparticles were measured by the software Image J; Fig. S1 shows that the diameters of Fe_3O_4@Au NPs (38.9 ± 2.9 nm) were a bit larger than Fe_3O_4 NPs (21.4 ± 3.3 nm) (about 200 nanoparticles were taken into calculation and particle size distributions of Fe_3O_4 NPs and Fe_3O_4@Au NPs are shown in Fig. S1C and Fig. S1D). In Fig. 2B, the distribution of Fe, Au, and Fe_3O_4@Au NPs in the same field of vision was characterized by EDS mapping; spherical nanoparticles could be observed in the vision of Fe_3O_4@Au NPs, suggesting that the Au NPs were successfully coated on the Fe_3O_4 NPs surface. As indicated in Fig. 2C, the formation of Fe_3O_4@Au NPs-S1 was verified by the UV-Vis absorption spectrum. The UV absorbance peak of Au NPs was obtained at 520 nm (curve a). Curve b showed that there was no characteristic adsorption peak of Fe_3O_4 NPs in the range of 200–700 nm. Moreover, after Au NPs were conjugated with Fe_3O_4 NPs, a new UV absorbance peak of Au NPs was obtained at 550 nm, showing a red shift compared with Au NPs, indicating that Fe_3O_4@Au nanocomposites were successfully synthesized (curve c). Two distinct absorbances of

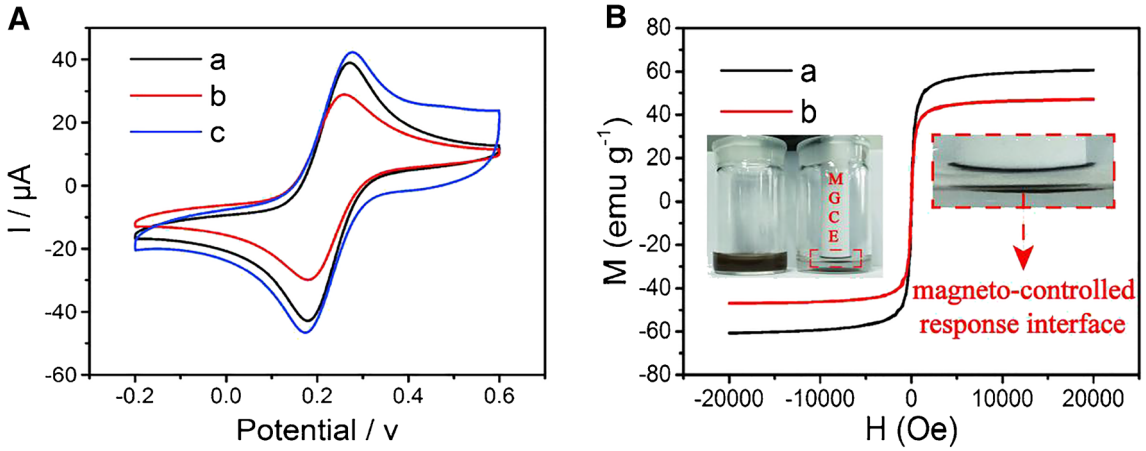

Fig. 1 Functions of the components. **A** Cyclic voltammograms with different materials. (a) Bare MGCE; (b) Fe_3O_4 NPs/MGCE; (c) Fe_3O_4@Au NPs/MGCE. **B** VSM analysis of (a) Fe_3O_4 NPs and (b) Fe_3O_4@Au NPs (the internal illustration on the left shows the rapid adsorption of MGCE to Fe_3O_4@Au NPs, the internal illustration on the right shows the magneto-controlled response interface on the surface of MGCE)

Fe_3O_4@Au NPs-S1 were observed at 260 nm and 550 nm (curve d); the peak at 260 nm is similar to that of the free S1 solution (curve e), which the S1 was successfully covalently linked with Fe_3O_4@Au NPs through Au-S bond (curve d). In addition, the zeta potential of Fe_3O_4@Au NPs-S1 (− 19.9 mV) decreased comparing with that of Fe_3O_4@Au NPs (22.3 mV) (Fig. 2D) due to the large number of negative groups contained in DNA (S1), further demonstrating the successful modification of S1.

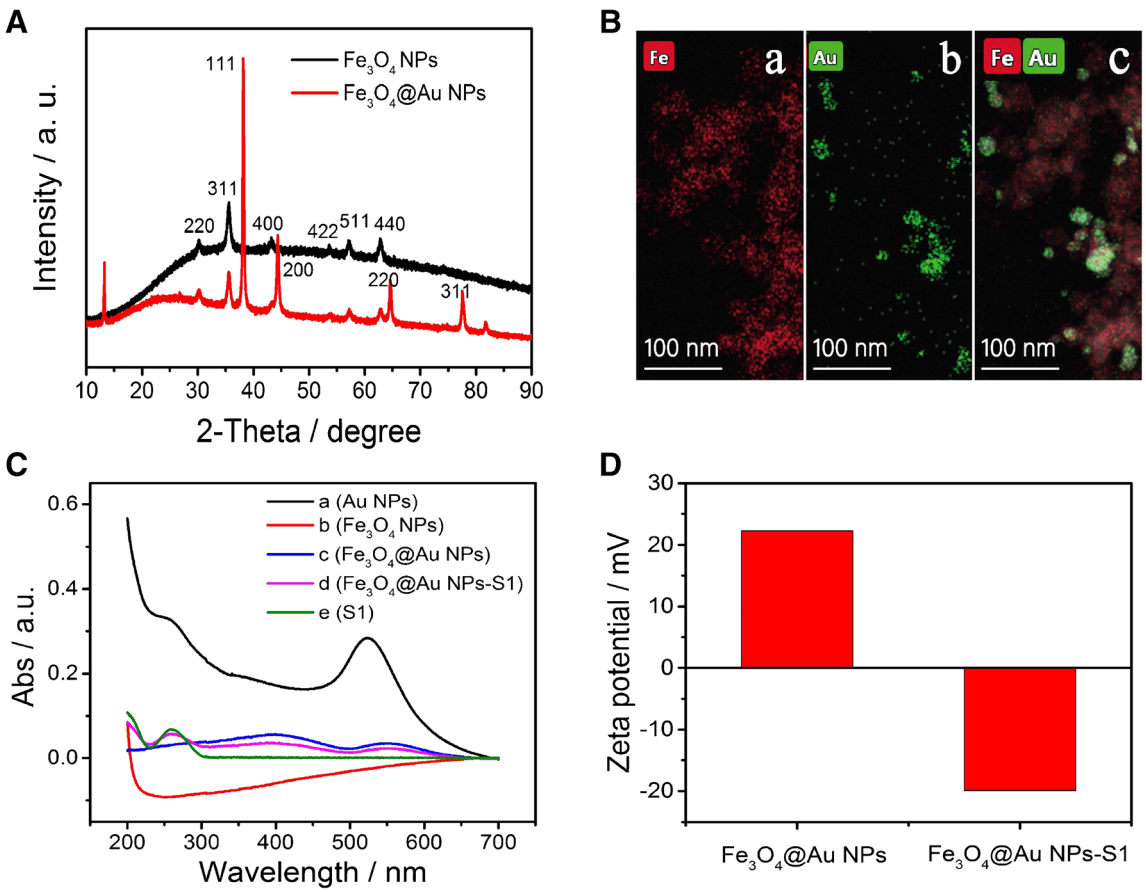

Fig. 2 Characterization of the materials. **A** The XRD spectra of Fe_3O_4 NPs and Fe_3O_4@Au NPs. **B** EDS mapping image for the distribution of Fe (a), Au (b), and Fe_3O_4@Au NPs (c) in the same field of vision. **C** UV-Vis spectra of Fe_3O_4@Au NPs-S1 (a, Au NPs; b, Fe_3O_4 NPs; c, Fe_3O_4@Au NPs; d, Fe_3O_4@Au NPs-S1, e, S1). **D** Zeta potential of Fe_3O_4@Au NPs and Fe_3O_4@Au NPs-S1

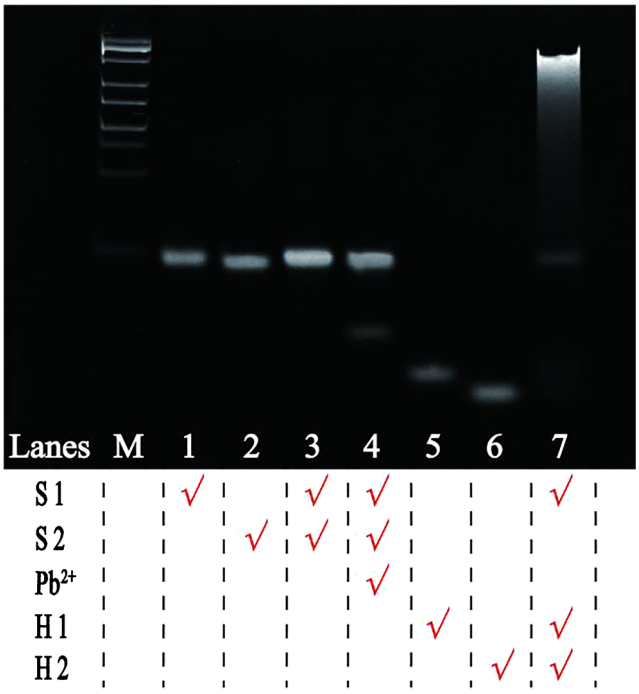

Fig. 3 Verification of analytical process by native-PAGE gel electrophoresis. Lane M: DNA marker; lane 1: S1; lane 2: S2; lane 3: S1 + S2; lane 4: S1 + S2 + Pb^{2+}; lane 5: H1; lane 6: H2; lane 7: S1 + H1 + H2 (HCR progress)

Feasibility analysis of the strategy

Native-PAGE gel electrophoresis analysis

Fifteen percent native-PAGE gel electrophoresis was utilized to characterize the different samples to verify the feasibility of the proposed biosensor in Pb^{2+} determination. As can be seen in Fig. 3, lane M represented DNA maker; lanes 1–2 were S1 and S2, respectively. Lane 3 was the band in the absence of Pb^{2+} and lane 4 was the band in the presence of Pb^{2+}. The S1 band became weak and an obvious band with faster migration could be seen in front in lane 4, indicating that the S1 was cleaved. Lane 5 and lane 6 were H1 and H2, respectively; after mixing S1, H1, and H2, there were obvious bands with slower migration at the bottom (lane 7), indicating that S1 could initiate the HCR so that the long dsDNA could be formed.

DPV analysis

The DPV was applied to evaluate the feasibility for the biosensor in detecting Pb^{2+}. As shown in Fig. 4A, when there was no Pb^{2+}, the S1 could not be cleaved, a small DPV response was obtained (curve a) due to the nonspecific adsorption of MB on ssDNA S1. When Pb^{2+} at the concentration of 1 μM was induced, S1 can be cleaved at the rA site by S2, a lower DPV response was obtained (curve b) resulting from the trace adsorption of MB on DNA fragments, I_T was decreased. Furthermore, when H1 and H2 were added, curve c showed an obvious current peak due to the HCR; as a result, I_0 was increased. When there was Pb^{2+} at the concentration of 1 μM, the electrochemical signal displayed a distinct decrease (curve d), which indicated that the S1 was cleaved and the initiator strand was separated from the reaction system, the HCR reaction cannot be triggered even in the presence of H1 and H2, revealing that the introduction of HCR is efficient in signal amplification in the proposed biosensor.

More specific, the electrochemical signal was detected with or without HCR, the current difference value ($\Delta I = I_0 - I_T$) was calculated. As shown in Fig. 4B, the ΔI treated with HCR increased nearly 6 times compared with the untreated ones in the condition of the Pb^{2+} that is at a low concentration of 5 nM.

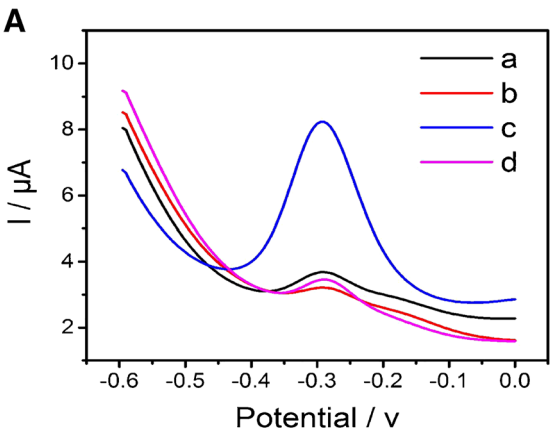

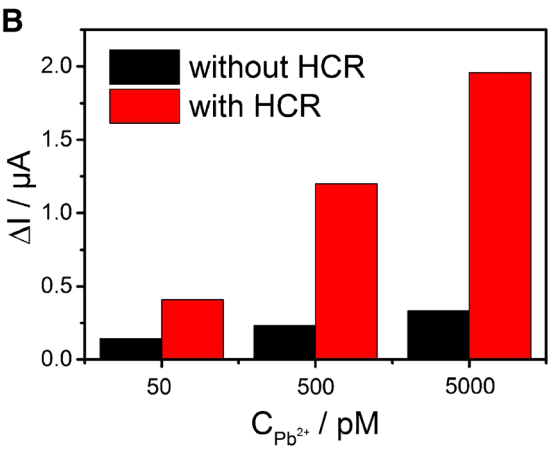

Fig. 4 **A** DPV curves of different condition: (a) Fe_3O_4@Au + S1 + MCH + S2 + MB, (b) Fe_3O_4@Au + S1 + MCH + S2 + Pb^{2+} + MB, (c) Fe_3O_4@Au + S1 + MCH + S2 + H1 + H2 + MB, (d) Fe_3O_4@Au + S1 + MCH + S2 + Pb^{2+} + H1 + H2 + MB. **B** The current difference value (ΔI) of Fe_3O_4@Au NPs-S1 incubated with S2 and different concentration of Pb^{2+} without HCR compared with that with HCR. ΔI was calculated by DPV difference of 0 pM Pb^{2+} with other concentration of Pb^{2+}

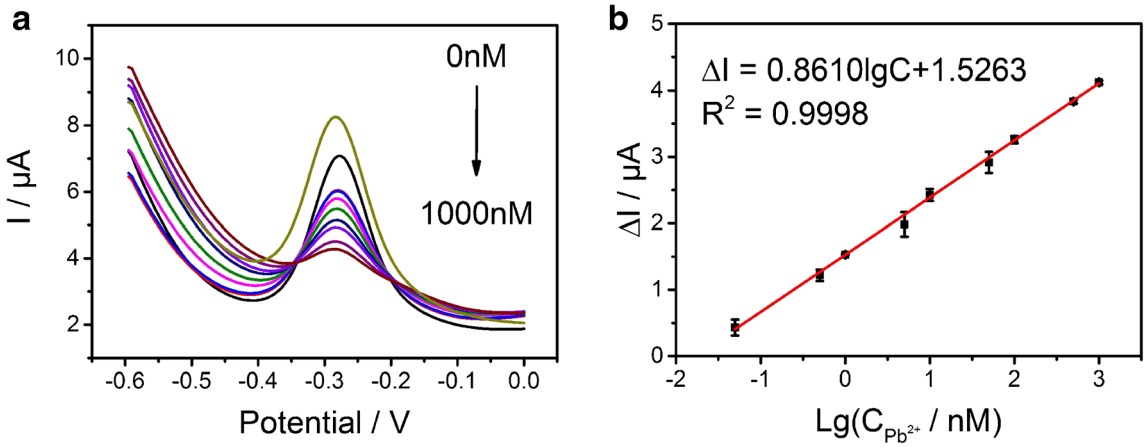

Fig. 5 **a** DPV images of the biosensor at the voltage of − 0.6~0.0 V after adding different concentrations of Pb^{2+}. The concentrations were 0 nM, 0.05 nM, 1 nM, 5 nM, 10 nM, 50 nM, 100 nM, 500 nM, and 1000 nM from top to bottom. **b** Calibration linear of DPV response to Pb^{2+}

Optimization of method

In order to obtain the optimum sensing performance, the following parameters were optimized: (a) the DNA density immobilized on Fe_3O_4@Au NPs, (b) the hybridization chain reaction time, (c) the molar ratio of S2 to S1, and (d) the reaction time of DNAzyme. Respective text and figures on optimizations are given in the Electronic Supporting Material. In short, the following experimental conditions were found to give the best results: the DNA immobilization density of 0.3 μM (Fig. S2A), the HCR time of 90 min (Fig. S2B), the molar ratio of S2 to S1 with 1:1 (Fig. S2C), and DNAzyme cleavage time with 40 min (Fig. S2D).

Electrochemical determination of Pb^{2+}

The determination performance of the fabricated biosensor was investigated by measuring Pb^{2+} at various concentrations. It can be obviously seen that with the increasing concentration of Pb^{2+}, the current response decreased (Fig. 5a). Figure 5 b shows the relationship between the ΔI (difference between electrochemical signal without Pb^{2+} and that with Pb^{2+}) and Pb^{2+} concentration, and a logarithmic calibration plot for Pb^{2+} determination from 0.05 nM to 1 μM was obtained, the linear regression equation was $\Delta I = 0.8610\lg C + 1.5263$ ($R^2 = 0.9998$). The limit of determination (LOD) was 15 pM (LOD = 3 s/d, where s is the standard deviation of the blank and d is the slope of the calibration curve). In addition, comparing with some of the previous report in detecting Pb^{2+} (Table S2), our proposed biosensor demonstrated a better performance.

Specificity and reproducibility of the biosensor

The selectivity of the biosensor for Pb^{2+} was estimated by detecting various metal ions including Zn^{2+}, Mg^{2+}, Fe^{3+}, Ag^{+}, Cu^{2+}, Cd^{2+}, Hg^{2+}, and Ca^{2+} (Fig. 6a). It could be seen that all the investigated possible interfering ions had

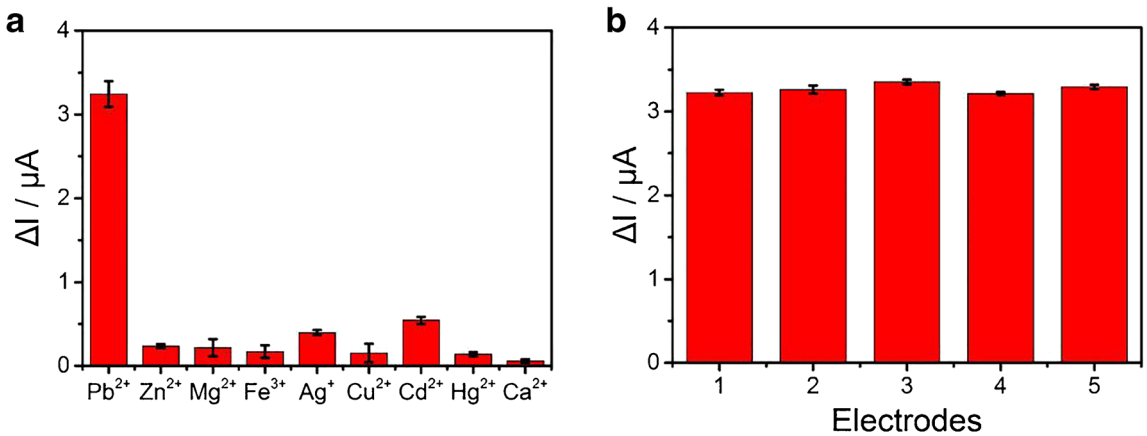

Fig. 6 **a** The responses of the proposed sensor to Pb^{2+} at the concentration of 100 nM and other metal ions at the concentration of 1 μM (Zn^{2+}, Mg^{2+}, Fe^{3+}, Ag^{+}, Cu^{2+}, Cd^{2+}, Hg^{2+}, Ca^{2+}). **b** The reproducibility of the five electrodes for the determination of 100 nM Pb^{2+}

Table 1 Results of Pb^{2+} determination ($n = 3$)

Sample	Measured (nM)	ICP-MS (nM)	Added Pb^{2+} (nM)	Founded Pb^{2+} (nM)	RSD ($n = 3$) (%)	Recovery (%)
			25	25.9 ± 0.7	2.54	103.6
Tap water	ND	ND	50	52.2 ± 1.2	2.21	104.4
			100	97.4 ± 3.1	3.15	97.4
			25	24.9 ± 0.9	3.51	99.6
Lake water	ND	ND	50	49.4 ± 2.0	4.13	98.8
			100	95.4 ± 1.4	1.51	95.4
Landfill leachate before treatment			25	115.8 ± 2.5	2.19	106.0
	89.3 ± 2.1	88.1	50	141.1 ± 2.6	1.84	103.6
			100	183.4 ± 7.7	4.19	94.1
Landfill leachate after treatment			25	55.4 ± 0.7	1.20	99.6
	30.5 ± 0.7	30.2	50	81.5 ± 1.5	1.84	101.4
			100	129.2 ± 4.2	3.27	98.7

ND not detected

The data are presented as mean value of three determinations ± standard deviations (SD)

almost no obvious effect on the response of this sensor to Pb^{2+}. The results demonstrated that the sensor has high selectivity toward Pb^{2+}. In addition, the reproducibility of the sensor was investigated by analyzing the same concentration of Pb^{2+} (100 nM) using five prepared electrodes under the same experimental condition (Fig. 6b). A relative standard deviation (RSD) of 3.45% was acquired.

Actual sample determination

To investigate the practical application effect of the proposed sensor, the determination for different concentrations of Pb^{2+} in different real water samples was conducted by standard addition method, including tap water, lake water, and landfill leachate before and after factory purify treatment. Before the test, four actual water samples were centrifuged at 12,000 rpm for 1 min and then filtered to remove the insoluble impurities. The Pb^{2+} in each real sample was determined by our method and ICP-MS, respectively. As shown in Table 1, the results of our sensor were in agreement with those determined using ICP-MS. Moreover, the RSD was below 4.19% and the recovery was from 94.1 to 106.0% in these real samples. According to these results, we can judge that the fabricated sensor possessed good precision and accuracy and has broad application prospects in environmental water samples.

Conclusion

We have established that a highly sensitive and selective electrochemical biosensor for Pb^{2+} was designed with a dual-amplification strategy. The Pb^{2+} and S2 could be circularly participated into the process of cutting S1 and the electrochemical signal was effectively reduced. Owing to the HCR and large surface of Fe_3O_4@Au NPs, mass of MB absorbed on dsDNA increased the electrochemical signal obviously, realizing the label-free determination. The significant current difference value enabled the highly sensitive determination of Pb^{2+}. Moreover, Fe_3O_4@Au NPs act as an excellent electrode material, not only making the proposed method convenient and simple for magnetic separation to purify the analysis system, but also realizing the free of electrode modification and enhancing the regeneration ability of the electrode. Considering the above obvious advantages, we preconceive that the proposed method has potential to be a sensitive, selective, and convenient platform for actual water sample analysis and has a broad application prospect in the field of environmental monitoring. Like many other electrochemical sensors, the major drawback of our sensor is the single signal output which may affect the accuracy and precision of the measurement results. We would explore the dual signal sensors in the future to improve the above performance of electrochemical sensors, especially the "on-off" dual signal sensors with high sensitivity.

Funding This work was supported by the National Natural Science Foundation of China (No. 81773681, 81572081, 21904069) and the Natural Science Foundation of Jiangsu Province (No. BK20190653). This work was also supported by Chinese Postdoctoral Science Foundation (No. 2019M661777, 2017M621789) and the Postdoctoral Science Foundation of Jiangsu (No. 2019K068, 2019Z176).

Compliance with ethical standards All experiments were performed in compliance with the relevant laws and institutional guidelines.

Conflict of interest The authors declare that they have no conflict interest.

References

1. Cai L-M, Wang Q-S, Luo J, Chen L-G, Zhu R-L, Wang S, Tang C-H (2019) Heavy metal contamination and health risk assessment for children near a large Cu-smelter in Central China. Sci Total Environ 650:725–733
2. Peng T, O'Connor D, Zhao B, Jin Y, Zhang Y, Tian L, Zheng N, Li X, Hou D (2019) Spatial distribution of lead contamination in soil and equipment dust at children's playgrounds in Beijing, China. Environ Pollut 245:363–370
3. Llop S, Aguinagalde X, Vioque J, Ibarluzea J, Guxens M, Casas M, Murcia M, Ruiz M, Amurrio A, Rebagliato M, Marina LS, Fernandez-Somoano A, Tardon A, Ballester F (2011) Prenatal exposure to lead in Spain: cord blood levels and associated factors. Sci Total Environ 409(11):2298–2305
4. He Q, Miller EW, Wong AP, Chang CJ (2006) A selective fluorescent sensor for detecting lead in living cells. J Am Chem Soc 128(29):9316–9317
5. Lu Y, Li X, Wang G, Tang W (2013) A highly sensitive and selective optical sensor for Pb^{2+} by using conjugated polymers and label-free oligonucleotides. Biosens Bioelectron 39(1):231–235
6. World Health Organization, Geneva (2011) WHO guidelines for drinking-water quality, 4th edn. Who, Geneva, pp 504–505
7. Bings NH, Bogaerts A, Broekaert JAC (2006) Atomic spectroscopy. Anal Chem 78/12:3917–3946
8. Serpell CJ, Rutte RN, Geraki K, Pach E, Martincic M, Kierkowicz M, De Munari S, Wals K, Raj R, Ballesteros B, Tobias G, Anthony DC, Davis BG (2016) Carbon nanotubes allow capture of krypton, barium and lead for multichannel biological X-ray fluorescence imaging. Nat Commun 7:13118
9. Luo R, Xiaohong S, Xu W, Zhang S, Zhuo X, Dong M (2017) Determination of arsenic and lead in single hair strands by laser ablation inductively coupled plasma mass spectrometry. Sci Rep 7:3421
10. Liu S, Wei W, Sun X, Wang L (2016) Ultrasensitive electrochemical DNAzyme sensor for lead ion based on cleavage-induced template-independent polymerization and alkaline phosphatase amplification. Biosens Bioelectron 83:33–38
11. Zhang Y, Xiao S, Li H, Liu H, Pang P, Wang H, Wu Z, Yang W (2016) A Pb^{2+}-ion electrochemical biosensor based on single-stranded DNAzyme catalytic beacon. Sensors Actuators B Chem 222:1083–1089
12. Wen Z-B, Liang W-B, Zhuo Y, Xiong C-Y, Zheng Y-N, Yuan R, Chai Y-Q (2017) An efficient target–intermediate recycling amplification strategy for ultrasensitive fluorescence assay of intracellular lead ions. Chem Commun 53(54):7525–7528
13. Yang Z, Wu H, Yi X, Tang J, Yun W, Han W, Chen X (2019) A universal converting strategy based on target-induced DNA nanoprobe conformational change for lead (II) ion assay. Biosens Bioelectron 144:111679
14. Zhang L, Deng H, Yuan R, Yuan Y (2019) Electrochemical lead(II) biosensor by using an ion-dependent split DNAzyme and a template-free DNA extension reaction for signal amplification. Microchim Acta 186:709
15. Hai H, Yang F, Li J (2014) Highly sensitive electrochemiluminescence "turn-on" aptamer sensor for lead(II) ion based on the formation of a G-quadruplex on a graphene and gold nanoparticles modified electrode. Microchim Acta 181(9): 893–901
16. Song X, Wang Y, Liu S, Zhang X, Wang J, Wang H, Zhang F, Yu J, Huang J (2019) A triply amplified electrochemical lead(II) sensor by using a DNAzyme and via formation of a DNA-gold nanoparticle network induced by a catalytic hairpin assembly. Mikrochim Acta 186/8:559
17. Zhu C, Zhu W, Xu L, Zhou X (2019) A label-free electrochemical aptasensor based on magnetic biocomposites with Pb^{2+}-dependent DNAzyme for the detection of thrombin. Anal Chim Acta 1047:21–27
18. Chen D, Zhang M, Ma M, Hai H, Li J, Yang S (2019) A novel electrochemical DNA biosensor for transgenic soybean detection based on triple signal amplification. Anal Chim Acta 1078:24–31
19. Han Q, Shen X, Zhu W, Zhu C, Zhou X, Jiang H (2016) Magnetic sensing film based on Fe_3O_4@Au-GSH molecularly imprinted polymers for the electrochemical detection of estradiol. Biosens Bioelectron 79:180–186
20. Zhu W, Jiang G, Xu L, Li B, Cai Q, Jiang H, Zhou X (2015) Facile and controllable one-step fabrication of molecularly imprinted polymer membrane by magnetic field directed self-assembly for electrochemical sensing of glutathione. Anal Chim Acta 886:37–47
21. Pang Y, Wan N, Shi L, Wang C, Sun Z, Xiao R, Wang S (2019) Dual-recognition surface-enhanced Raman scattering(SERS)biosensor for pathogenic bacteria detection by using vancomycin-SERS tags and aptamer-Fe_3O_4@Au. Anal Chim Acta 1077:288–296
22. Premaratne G, Dharmaratne AC, Al Mubarak ZH, Mohammadparast F, Andiappan M, Krishnan S (2019) Multiplexed surface plasmon imaging of serum biomolecules: Fe_3O_4@Au Core/shell nanoparticles with plasmonic simulation insights. Sens Actuators B: Chem 299:126956
23. Choi HMT, Beck VA, Pierce NA (2014) Next-generation in situ hybridization chain reaction: higher gain, lower cost, greater durability. ACS Nano 8/5:4284–4294
24. Zhou Q, Lin Y, Zhang K, Li M, Tang D (2018) Reduced graphene oxide/$BiFeO_3$ nanohybrids-based signal-on photoelectrochemical sensing system for prostate-specific antigen detection coupling with magnetic microfluidic device. Biosens Bioelectron 101:146–152
25. Chu Y, Deng A-P, Wang W, Zhu J-J (2019) Concatenated catalytic hairpin assembly/hyperbranched hybridization chain reaction based enzyme-free signal amplification for the sensitive photoelectrochemical detection of human telomerase RNA. Anal Chem 91(5):3619–3627
26. Chen X, Huang J, Zhang S, Mo F, Shasha S, Li Y, Fang L, Deng J, Huang H, Luo Z, Zheng J (2019) Electrochemical biosensor for DNA methylation detection through hybridization chain-amplified reaction coupled with a tetrahedral DNA nanostructure. ACS Appl Mater Interfaces 11(4):3745–3752
27. Hou T, Li W, Liu X, Li F (2015) Label-free and enzyme-free homogeneous electrochemical biosensing strategy based on hybridization chain reaction: a facile, sensitive, and highly specific MicroRNA assay. Anal Chem 87(22):11368–11374
28. Rohs R, Sklenar H, Lavery R, Röder B (2000) Methylene blue binding to DNA with alternating GC base sequence: a modeling study. J Am Chem Soc 122(12):2860–2866
29. Drummond TG, Hill MG and Barton JK (2003) Electrochemical DNA sensors. Nat Biotechnol 21/10:1192–1199
30. Baker BR, Lai RY, Wood MCS, Doctor EH, Heeger AJ, Plaxco KW (2006) An electronic, Aptamer-based small-molecule sensor for the rapid, label-free detection of cocaine in adulterated samples and biological fluids. J Am Chem Soc 128(10):3138–3139
31. Chen J, Zhang J, Wang K, Lin X, Huang L, Chen G (2008) Electrochemical biosensor for detection of BCR/ABL fusion gene using locked nucleic acids on 4-aminobenzenesulfonic acid-modified glassy carbon electrode. Anal Chem 80(21):8028–8034
32. Xuan F, Luo X, Hsing I-M (2012) Ultrasensitive solution-phase electrochemical molecular beacon-based DNA detection with signal amplification by exonuclease III-assisted target recycling. Anal Chem 84(12):5216–5220

33. Wu J, Yang Z, Chen N, Zhu W, Hong J, Huang C, Zhou X (2015) Vanillin-molecularly targeted extraction of stir bar based on magnetic field induced self-assembly of multifunctional Fe_3O_4@polyaniline nanoparticles for detection of vanilla-flavor enhancers in infant milk powders. J Colloid Interface Sci 442:22–29
34. Zhang H, Ma L, Li P, Zheng J (2016) A novel electrochemical immunosensor based on nonenzymatic Ag@Au-Fe_3O_4 nanoelectrocatalyst for protein biomarker detection. Biosens Bioelectron 85:343–350
35. Shen X, Ge Z, Pang Y (2015) Conjugating folate on superparamagnetic Fe_3O_4@Au nanoparticles using click chemistry. J Solid State Chem 222:37–43